Mechanics of Advanced Materials and Structures
Publication details, including instructions for authors and subscription information:
http://www.tandfonline.com/loi/umcm20

Hybrid Graded Element Model for Nonlinear Functionally Graded Materials

Hui Wang [a b], Leilei Cao [b c] & Qing-Hua Qin [b]

[a] College of Civil Engineering and Architecture, Henan University of Technology, Zhengzhou, China

[b] School of Engineering, Australian National University, Canberra, ACT, Australia

[c] Key Laboratory for Highway Construction Technology and Equipment of Ministry of Education, Chang'an University, Xi'an, China

Accepted author version posted online: 13 Apr 2012.Version of record first published: 05 Sep 2012.

To cite this article: Hui Wang, Leilei Cao & Qing-Hua Qin (2012): Hybrid Graded Element Model for Nonlinear Functionally Graded Materials, Mechanics of Advanced Materials and Structures, 19:8, 590-602

To link to this article: http://dx.doi.org/10.1080/15376494.2011.563411

Mechanics of Advanced Materials and Structures, 19:590–602, 2012

ISSN: 1537-6494 print / 1537-6532 online
DOI: 10.1080/15376494.2011.563411

Taylor & Francis
Taylor & Francis Group

Hybrid Graded Element Model for Nonlinear Functionally Graded Materials

Hui Wang,[1,2] Leilei Cao,[2,3] and Qing-Hua Qin[2]

[1]*College of Civil Engineering and Architecture, Henan University of Technology, Zhengzhou, China*
[2]*School of Engineering, Australian National University, Canberra, ACT, Australia*
[3]*Key Laboratory for Highway Construction Technology and Equipment of Ministry of Education, Chang'an University, Xi'an, China*

A hybrid graded element model is developed in this article for solving the heat conduction problem of nonlinear functionally graded materials (FGMs), whose material properties not only vary spatially but also are temperature dependent. In the proposed approach, both Kirchhoff transformation and iterative method are introduced to deal with the nonlinear term in the heat conduction equation of nonlinear FGMs. Then, the graded element is formulated based on two sets of independent temperature fields. One is the intra-element temperature field, which is defined within the element domain and constructed by a linear combination of fundamental solutions; the other is the frame field, which is defined on the element boundary only and used as the boundary interpolation functions of the element to ensure the field continuity over the inter-element boundary. This model can simulate the graded material properties naturally due to the inherent properties of fundamental solutions, which are employed in constructing the graded element. Moreover, a multi-subdomain method is developed to deal with the problem with different materials. Finally, the performance of the proposed method is assessed by several benchmark examples. The results are in excellent agreement with the analytical solutions.

Keywords graded element model, nonlinear functionally graded materials, hybrid FEM, heat conduction

1. INTRODUCTION

Functionally graded materials (FGMs) are new advanced heat resistant materials that are formed using modern technologies and used in advanced structures. The concept of FGM is to make a composite material by varying the microstructure from one material to another material with a specific gradient. Since FGMs are expected to be used under high temperature and high heating rate environment, it is necessary to understand their thermal behavior. However, thermal analysis of FGMs is far more difficult than that of homogeneous materials due to their possible temperature-dependent and continuously varying material properties.

Two typical finite element models (the stepwise constant model and the Gauss point sampling model) can be found in the literatures to simulate physical behavior of FGMs. In the stepwise constant model [1, 2], the element rows are aligned along the gradient direction and the material property of each row of the homogeneous elements is taken to be the property at the centroid of the element, and the material gradient is achieved by highly refined element mesh. In the Gauss point sampling model [3–5], the material gradient is directly sampled by assigning corresponding material properties at the Gauss integration points. In addition, other types of numerical methods, including finite element method (FEM) [5, 6], boundary element method (BEM) [7, 8], or dual reciprocity BEM [9, 10], the method of fundamental solution [11, 12] and meshless methods, which includes local Petrov-Galerkin method [13] and local boundary integral equation method [14], have also been used to analyze thermal response of FGMs. Most of them used an exponential variation of material constants along Cartesian coordinates and the heat conductivity is assumed to be independent of temperature. As a consequence, the problem can be modeled as a linear FGM problem. The linearity, however, is not preserved in many practical engineering problems due to the temperature-dependence of heat conductivity.

In this article, a nonlinear graded element model for the heat conduction problem of functionally graded materials whose material properties vary not only with Cartesian coordinates, but also with temperature is discussed. The study extends the hybrid fundamental solution based finite element method (HFS-FEM) presented in [15, 16] to the case of nonlinear FMGs. HFS-FEM is a newly developed hybrid finite element formulation with fundamental solutions as intra-element interpolation. It inherits all advantages of the hybrid Trefftz FEM (HT-FEM) over the conventionally FEM and BEM (details in references [17–20]) and removes the difficulty encountered in constructing and

Received 8 February 2010; accepted 25 September 2010.
Address correspondence to Qing-Hua Qin, School of Engineering, Australian National University, Canberra, ACT 0200, Australia. E-mail: qinghua.qin@anu.edu.au

selecting T-functions. In the present hybrid graded model, a linear combination of the fundamental solution for functionally graded materials at different source points is used to approximate the field variable within the element and an independent frame field defined along the element boundary is employed to guarantee the inter-element continuity. A variational functional is used to generate the final stiffness equation and establish a linkage between the boundary frame field and internal field within the element level. The proposed graded element formulation can incorporate the graded material property at the element level, so it is more natural than the conventional homogeneous elements model and Gauss point sampling model mentioned above. In the analysis, both Kirchhoff transformation and iterative method are employed to deal with the nonlinear thermal conductivity, which is the function of coordinates and unknown temperature field. For the functionally graded bi-material, a multi-subdomain method is developed to guarantee the continuity of temperature and heat flux on the interface of the two materials.

The article begins with a brief description of heat conduction problems in FGMs in Section 2. Then, a detailed derivation of the proposed nonlinear graded element and the corresponding algorithm is described in Section 3, to provide an initial insight on this new finite element model. Section 4 introduces the method to deal with the nonlinear functionally graded bi-material. Several numerical examples representing different kinds of nonlinear FGMs are also presented in Section 4 to demonstrate the efficiency of the proposed algorithm, and some concluding remarks are given in Section 5.

2. STATEMENT OF HEAT CONDUCTION PROBLEMS IN NONLINEAR FGM

2.1. Basic Formulations

Consider a two-dimensional (2-D) heat conduction problem defined in an anisotropic inhomogeneous media:

$$\sum_{i,j=1}^{2} \frac{\partial}{\partial X_i}(\tilde{K}_{ij}(\mathbf{X}, u)\frac{\partial u(\mathbf{X})}{\partial X_j}) = 0 \quad \forall \mathbf{X} \in \Omega. \tag{1}$$

For an inhomogeneous nonlinear functionally graded material, we assume the thermal conductivity varies exponentially with position vector and also be a function of temperature, that is,

$$\tilde{K}_{ij}(\mathbf{X}, u) = \alpha(u) K_{ij} \exp(2\boldsymbol{\beta} \cdot \mathbf{X}), \tag{2}$$

where $\alpha(u) > 0$ is a function of temperature, which may be different for different materials (see examples 1 and 2 for details), the vector $\boldsymbol{\beta} = (\beta_1, \beta_2)$ is a dimensionless graded parameter and matrix $\mathbf{K} = [K_{ij}]_{1 \le i,j \le 2}$ is a symmetric, positive-definite constant matrix ($K_{12} = K_{21}$, $\det \mathbf{K} = K_{11}K_{22} - K_{12}^2 > 0$).

The boundary conditions are as follows:

- Dirichlet boundary condition:

$$u = \bar{u} \quad \text{on } \Gamma_u. \tag{3}$$

- Neumann boundary condition:

$$q = -\sum_{i,j=1}^{2} \tilde{K}_{ij} \frac{\partial u}{\partial X_j} n_i = \bar{q} \quad \text{on } \Gamma_q, \tag{4}$$

where $\tilde{K}_{ij}$ denotes the thermal conductivity, which is the function of spatial variable $\mathbf{X}$ and unknown temperature field u. q represents the boundary heat flux. n_j is the direction cosine of the unit outward normal vector $\mathbf{n}$ to the boundary $\Gamma = \Gamma_u \cup \Gamma_q$. $\bar{u}$ and $\bar{q}$ are specified functions on the related boundaries, respectively.

2.2. Kirchhoff Transformation and Iterative Method

Two methods are employed here to deal with the nonlinear term $\alpha(u)$, one is Kirchhoff transformation [11] and another is the iterative method.

2.2.1. Kirchhoff Transformation

The Kirchhoff transformation is shown as follows:

$$\boldsymbol{\Psi}(u) = \psi(u(\mathbf{X})) = \int \alpha(u) du. \tag{5}$$

Making use of Eq. (5), Eq. (1) reduces to:

$$\sum_{i,j=1}^{2} \frac{\partial}{\partial X_i}\left(K_{ij}^*(\mathbf{X}) \frac{\partial \Psi(\mathbf{X})}{\partial X_j}\right) = 0 \quad \forall \mathbf{X} \in \Omega, \tag{6}$$

where

$$K_{ij}^*(\mathbf{X}) = K_{ij} \exp(2\boldsymbol{\beta} \cdot \mathbf{X}). \tag{7}$$

Substituting Eq. (7) into Eq. (6) yields:

$$\left[\sum_{i,j=1}^{2} K_{ij} \frac{\partial^2 \Psi(\mathbf{X})}{\partial X_i \partial X_j} + 2\boldsymbol{\beta} \cdot (\mathbf{K} \nabla \Psi(\mathbf{X}))\right] \exp(2\boldsymbol{\beta} \cdot \mathbf{X}) = 0, \quad \mathbf{X} \in \Omega, \tag{8}$$

where

$$u = \psi^{-1}(\Psi). \tag{9}$$

It should be mentioned that the inverse of Ψ in Eq. (9) exists since $\alpha(u) > 0$.

The fundamental solution to Eq. (8) in two dimensions can be expressed as [11, 21]:

$$N(\mathbf{X}, \mathbf{X}_s) = -\frac{K_0(\kappa R)}{2\pi\sqrt{\det \mathbf{K}}} \exp\{-\boldsymbol{\beta} \cdot (\mathbf{X} + \mathbf{X}_s)\}, \tag{10}$$

where $\kappa = \sqrt{\boldsymbol{\beta} \cdot \mathbf{K}\boldsymbol{\beta}}$, R is the geodesic distance defined as $R = R(\mathbf{X}, \mathbf{X}_s) = \sqrt{\mathbf{r} \cdot \mathbf{K}^{-1}\mathbf{r}}$ and $\mathbf{r} = \mathbf{r}(\mathbf{X}, \mathbf{X}_s) = \mathbf{X} - \mathbf{X}_s$, in which $\mathbf{X}$ and $\mathbf{X}_s$ denote the observing field point and source point in the infinite domain, respectively. K_0 is the modified Bessel function of the second kind of zero order. For isotropic materials, $K_{12} = K_{21} = 0$, $K_{11} = K_{22} = k_0 > 0$, then the fundamental solution given by (10) reduces to:

$$N(\mathbf{X}, \mathbf{X}_s) = -\frac{K_0(\kappa R)}{2\pi k_0} \exp\{-\beta \cdot (\mathbf{X} + \mathbf{X}_s)\}, \tag{11}$$

which agrees with the result in [22].

Under the Kirchhoff transformation, the boundary conditions (3) and (4) are transformed into the corresponding boundary conditions in terms of Ψ:

$$\Psi = \psi(\bar{u}) \quad \text{on } \Gamma_u, \tag{12}$$

$$p = -\sum_{i,j=1}^{2} K_{ij}^{*} \frac{\partial \Psi}{\partial X_j} n_i = -\sum_{i,j=1}^{2} \tilde{K}_{ij} \frac{\partial u}{\partial X_j} n_i = q = \bar{q} \quad \text{on } \Gamma_q. \tag{13}$$

Therefore, by Kirchhoff transformation, the original nonlinear heat conduction equation (1), in which the heat conductivity is a function of coordinate X and unknown function u, can be transformed into the linear equation (6), in which the heat conductivity is just a function of coordinate X. At the same time, the field variable becomes Ψ in Eq. (6), rather than u in Eq. (1). The boundary conditions (3) and (4) are correspondingly transformed into Eqs. (12) and (13). Once Ψ is determined, the temperature solution u can be found by the reversion of transformation (9), i.e., $u = \psi^{-1}(\Psi)$.

2.2.2. *Iterative Method*

Since the heat conductivity depends on the unknown function u, an iterative procedure is employed for determining the temperature distribution. The algorithm is given as follows:

Assume an initial temperature u^0.

Calculate the heat conductivity in Eq. (2) using u^0.

Solve the boundary value problem defined by Eqs. (1)–(4) for the temperature u.

Define the convergent criterion $|u - u^0| < \delta$ ($\delta = 10^{-6}$ in our analysis). If the criterion is satisfied, output the result and terminate the process. If not satisfied, go to the next step.

Update u^0 with u.

Go to step 2.

3. GENERATION OF GRADED ELEMENT

In this section, an element formulation is presented to deal with materials with continuous variation of physical properties. Such an element model is usually known as a hybrid graded element that can be used for solving the boundary value problem defined in Eqs. (6) and (12)–(13).

The proposed approach is based on a hybrid finite element formulation in which fundamental solutions are taken as intra-element interpolation functions (HFS-FEM for short) [16]. Similar to HT-FEM, the main idea of HFS-FEM is to establish an appropriate hybrid finite element formulation whereby intra-element continuity is enforced on a nonconforming intra-element field formed by a linear combination of fundamental solutions at points outside the element domain under consideration, while an auxiliary frame field is independently defined on the element boundary to enforce the field continuity across inter-element boundaries. But unlike in the HT-FEM, the intra-element fields are constructed based on the fundamental solution, rather than T-functions. Consequently, a variational functional corresponding to the new trial function is required to derive the related stiffness matrix equation. As was done in conventional FEM, the solution domain is divided into sub-domains or elements. For a particular element, say element e, its domain is denoted by Ω_e and bounded by Γ_e. Since a nonconforming function is used for modeling an intra-element field, additional continuities are usually required over the common boundary Γ_{Ief} between any two adjacent elements 'e' and 'f' (see Figure 1) [23]:

$$\left.\begin{aligned} \Psi_e &= \Psi_f \,(\text{conformity}) \\ p_e + p_f &= 0 \,(\text{reciprocity}) \end{aligned}\right\} \quad \text{on } \Gamma_{Ief} = \Gamma_e \cap \Gamma_f, \tag{14}$$

in the proposed hybrid FE approach.

3.1. Nonconforming Intra-Element Field

For a particular element, say element e, which occupies subdomain Ω_e, the field variable within the element is extracted

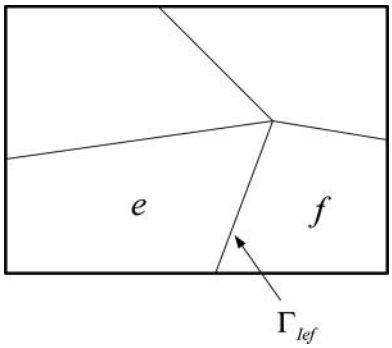

FIG. 1. Illustration of continuity between two adjacent elements 'e' and 'f'.

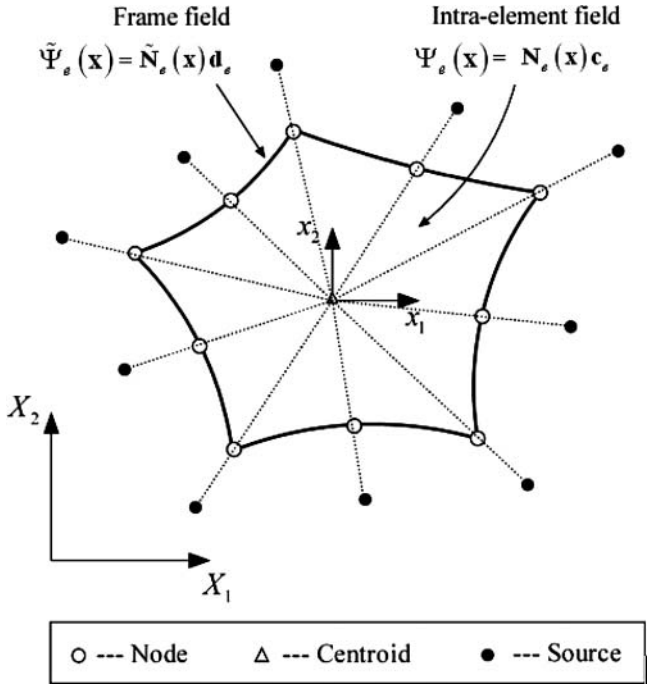

FIG. 2. Intra-element field, frame field in a particular element in HFS-FEM, and the generation of source points for a particular element.

from a linear combination of fundamental solutions centered at different source points (see Figure 2), that is,

$$\Psi_e(\mathbf{x}) = \sum_{j=1}^{n_s} N_e(\mathbf{x}, \mathbf{y}_j)\, c_{ej} = \mathbf{N}_e(\mathbf{x})\,\mathbf{c}_e \quad \forall \mathbf{x} \in \Omega_e, \mathbf{y}_j \notin \Omega_e, \tag{15}$$

where c_{ej} is undetermined coefficients and n_s is the number of virtual sources outside the element e. $N_e(\mathbf{x}, \mathbf{y}_j)$ is the required fundamental solution expressed in terms of local element coordinates (x_1, x_2), instead of global coordinates (X_1, X_2) (see Figure 2). Obviously, Eq. (15) analytically satisfies the heat conduction equation (8) due to the inherent property of $N_e(\mathbf{x}, \mathbf{y}_j)$.

The fundamental solution for FGM (N_e in Eq. (15)) is used to approximate the intra-element field in FGM. It is well known that the fundamental solution represents the field generated by a concentrated unit source acting at a point, so the smooth variation of material properties throughout an element can be achieved by this inherent property, instead of the stepwise constant approximation, which has been frequently used in the conventional FEM. For example, Figure 3 illustrates the difference between the two models when the thermal conductivity varies along direction X_2 in isotropic material.

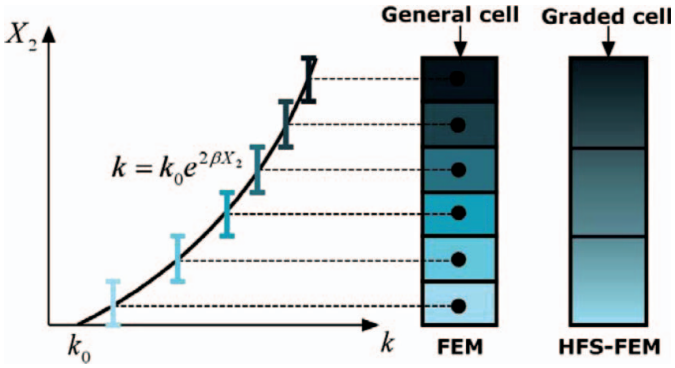

FIG. 3. Comparison of computational cell in the conventional FEM and the proposed HFS-FEM. (Color figure available online.)

Note that the thermal conductivity in Eq. (7) is defined in the global coordinate system. When contriving the intra-element field for each element, this formulation has to be transferred into the local element coordinate system defined at the center of the element, the graded matrix $\mathbf{K}^*$ in Eq. (7) can then be expressed by:

$$\mathbf{K}_e^*(\mathbf{x}) = \mathbf{K}_C \exp(2\boldsymbol{\beta} \cdot \mathbf{x}), \tag{16}$$

for a particular element e, where $\mathbf{K}_C$ denotes the value of conductivity at the centroid of each element and can be calculated as follows:

$$\mathbf{K}_C = \mathbf{K} \exp(2\boldsymbol{\beta} \cdot \mathbf{X}_c), \tag{17}$$

where $\mathbf{X}_c$ is the global coordinate of the element centroid.

Accordingly, the matrix $\mathbf{K}_C$ is used to replace $\mathbf{K}$ (see Eq. (10)) in the formulation of fundamental solution for FGM and to construct an intra-element field in the coordinate system local to element.

In practice, the generation of virtual sources is usually done by means of the following formulation employed in the method of fundamental solution (MFS) [24, 25]:

$$\mathbf{y} = \mathbf{x}_b + \mu\,(\mathbf{x}_b - \mathbf{x}_c), \tag{18}$$

where μ is a dimensionless coefficient ($\mu = 2.5$ in our analysis [16]), $\mathbf{x}_b$ and $\mathbf{x}_c$ are, respectively, boundary point and geometrical centroid of the element. For a particular element shown in Figure 2, we can use the nodes of element to generate related source points.

The corresponding normal heat flux on Γ_e is given by:

$$p_e = -\mathbf{K}_e^* \frac{\partial \Psi_e}{\partial X_j} n_i = \mathbf{Q}_e \mathbf{c}_e, \tag{19}$$

where

$$\mathbf{Q}_e = -\mathbf{K}_e^* \frac{\partial \mathbf{N}_e}{\partial X_j} n_i = -\mathbf{A}\mathbf{K}_e^* \mathbf{T}_e \tag{20}$$

with

$$\mathbf{T}_e = [\,\mathbf{N}_{e,1} \quad \mathbf{N}_{e,2}\,]^{\mathrm{T}},\ \mathbf{A} = [\,n_1 \quad n_2\,]. \tag{21}$$

3.2. Auxiliary Conforming Frame Field

In order to enforce the conformity on the field variable u, for instance, $\Psi_e = \Psi_f$ on $\Gamma_e \cap \Gamma_f$ of any two neighboring elements e and f, an auxiliary inter-element frame field $\tilde{\Psi}$ is used and expressed in terms of nodal degrees of freedom (DOF), $\mathbf{d}$, as used in the conventional finite elements as:

$$\tilde{\Psi}_e(\mathbf{x}) = \tilde{\mathbf{N}}_e(\mathbf{x})\,\mathbf{d}_e, \tag{22}$$

which is independently assumed along the element boundary, where $\tilde{\mathbf{N}}_e$ represents the conventional FE interpolating functions. For example, a simple interpolation of the frame field on the side with three nodes of a particular element can be given in the form:

$$\tilde{\Psi} = \tilde{N}_1\Psi_1 + \tilde{N}_2\Psi_2 + \tilde{N}_3\Psi_3, \tag{23}$$

where $\tilde{N}_i$ $(i = 1, 2, 3)$ stands for shape functions in terms of natural coordinate ξ defined in Figure 4.

3.3. Modified Variational Principle and Stiffness Equation

3.3.1. Modified Variational Functional

For the boundary value problem defined in Eqs. (6) and (12)–(13), since the stationary conditions of the traditional potential or complementary variational functional cannot guarantee the satisfaction of the inter-element continuity condition required in the proposed HFS-FE model, a modified potential functional is developed as follows [16]:

$$\begin{aligned}\Pi_m &= \sum_e \Pi_{me} \\ &= \sum_e \left\{ -\int_{\Omega_e} \frac{1}{2} K_{ij}^* \Psi_{,i} \Psi_{,j} \mathrm{d}\Omega - \int_{\Gamma_{qe}} \bar{q}\tilde{\Psi}\mathrm{d}\Gamma \right. \\ &\quad \left. + \int_{\Gamma_e} (\tilde{\Psi} - \Psi) p \mathrm{d}\Gamma \right\},\end{aligned} \tag{24}$$

in which the governing equation (6) is assumed to be satisfied, a priori, in deriving the HFS-FE model (for convenience, the repeated subscript indices stand for summation convention). The boundary Γ_e of a particular element consists of the following parts:

$$\Gamma_e = \Gamma_{ue} \cup \Gamma_{qe} \cup \Gamma_{Ie}, \tag{25}$$

where Γ_{Ie} represents the inter-element boundary of the element 'e' shown in Figure 1.

The stationary condition of the functional (24) can lead to the governing equation (Euler equation), boundary conditions, and continuity conditions, details of the derivation can refer to [16, 17].

3.3.2. Stiffness Equation

Having independently defined the intra-element field and frame field in a particular element (see Figure 2), the next step is to generate the element stiffness equation through a variational approach and to establish a linkage between the two independent fields.

The variational functional Π_e corresponding to a particular element e of the present problem can be written as:

$$\Pi_{me} = -\frac{1}{2}\int_{\Omega_e} K_{ij}^* \Psi_{,i}\Psi_{,j}\mathrm{d}\Omega - \int_{\Gamma_{qe}} \bar{q}\tilde{\Psi}\mathrm{d}\Gamma + \int_{\Gamma_e} p(\tilde{\Psi} - \Psi)\mathrm{d}\Gamma. \tag{26}$$

Applying the Gauss theorem to the above functional, we have the following functional for the HFS-FE model:

$$\begin{aligned}\Pi_{me} = \frac{1}{2}\left[\int_{\Gamma_e} p\Psi\mathrm{d}\Gamma + \int_{\Omega_e} \Psi(K_{ij}^* u_{,i})_{,j}\mathrm{d}\Omega\right] - \int_{\Gamma_{qe}} \bar{q}\tilde{\Psi}\mathrm{d}\Gamma \\ + \int_{\Gamma_e} p(\tilde{\Psi} - \Psi)\mathrm{d}\Gamma.\end{aligned} \tag{27}$$

Considering the governing equation (6), we finally have the functional defined on the element boundary only:

$$\Pi_{me} = -\frac{1}{2}\int_{\Gamma_e} p\Psi\mathrm{d}\Gamma - \int_{\Gamma_{qe}} \bar{q}\tilde{\Psi}\mathrm{d}\Gamma + \int_{\Gamma_e} p\tilde{\Psi}\mathrm{d}\Gamma, \tag{28}$$

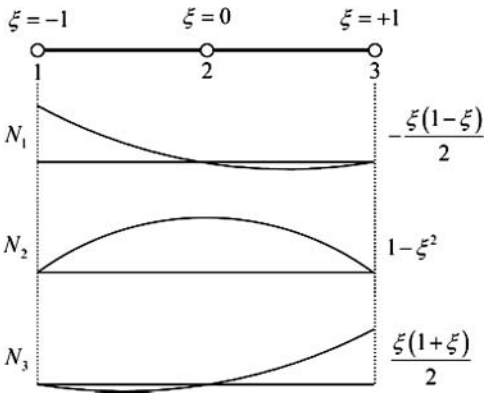

FIG. 4. Typical quadratic interpolation for the frame field.

which yields by substituting Eqs. (15), (19), and (22) into the functional (28):

$$\Pi_{me} = -\frac{1}{2}\mathbf{c}_e^{\mathrm{T}}\mathbf{H}_e\mathbf{c}_e - \mathbf{d}_e^{\mathrm{T}}\mathbf{g}_e + \mathbf{c}_e^{\mathrm{T}}\mathbf{G}_e\mathbf{d}_e, \tag{29}$$

with

$$\mathbf{H}_e = \int_{\Gamma_e} \mathbf{Q}_e^{\mathrm{T}}\mathbf{N}_e \mathrm{d}\Gamma \quad \mathbf{G}_e = \int_{\Gamma_e} \mathbf{Q}_e^{\mathrm{T}}\tilde{\mathbf{N}}_e \mathrm{d}\Gamma \quad \mathbf{g}_e = \int_{\Gamma_{qe}} \tilde{\mathbf{N}}_e^{\mathrm{T}}\bar{\mathrm{q}} \mathrm{d}\Gamma. \tag{30}$$

Next, to enforce inter-element continuity on the common element boundary, the unknown vector $\mathbf{c}_e$ should be expressed in terms of nodal DOF $\mathbf{d}_e$. The minimization of the functional Π_e with respect to $\mathbf{c}_e$ and $\mathbf{d}_e$, respectively, yields:

$$\begin{aligned} \frac{\partial \Pi_{me}}{\partial \mathbf{c}_e^{\mathrm{T}}} &= -\mathbf{H}_e\mathbf{c}_e + \mathbf{G}_e\mathbf{d}_e = \mathbf{0} \\ \frac{\partial \Pi_{me}}{\partial \mathbf{d}_e^{\mathrm{T}}} &= \mathbf{G}_e^{\mathrm{T}}\mathbf{c}_e - \mathbf{g}_e = \mathbf{0}, \end{aligned} \tag{31}$$

from which the optional relationship between $\mathbf{c}_e$ and $\mathbf{d}_e$, and the stiffness equation can be produced in the form:

$$\mathbf{c}_e = \mathbf{H}_e^{-1}\mathbf{G}_e\mathbf{d}_e \quad \text{and} \quad \mathbf{K}_e\mathbf{d}_e = \mathbf{g}_e, \tag{32}$$

where $\mathbf{K}_e = \mathbf{G}_e^{\mathrm{T}}\mathbf{H}_e^{-1}\mathbf{G}_e$ stands for the element stiffness matrix.

3.4. Recovery of Rigid-Body Motion

Considering the physical definition of the fundamental solution, it's necessary to recover the missing rigid-body motion modes from the above results.

Following the method presented in [18], the missing rigid-body motion can be recovered by writing the internal potential field of a particular element e as:

$$\Psi_e = \mathbf{N}_e\mathbf{c}_e + c_0, \tag{33}$$

where the undetermined rigid-body motion parameter c_0 can be calculated using the least square matching of Ψ_e and $\tilde{\Psi}_e$ at element nodes:

$$\sum_{i=1}^{n} (\mathbf{N}_e\mathbf{c}_e + c_0 - \tilde{\Psi}_e)^2\big|_{\text{node } i} = \min, \tag{34}$$

which finally gives

$$c_0 = \frac{1}{n}\sum_{i=1}^{n} \Delta\Psi_{ei}, \tag{35}$$

in which $\Delta\Psi_{ei} = (\tilde{\Psi}_e - \mathbf{N}_e\mathbf{c}_e)|_{\text{node } i}$ and n is the number of element nodes.

Once the nodal field is determined by solving the final stiffness equation, the coefficient vector $\mathbf{c}_e$ can be evaluated from Eq. (32), and then c_0 is evaluated from Eq. (35). Finally, the potential field Ψ at any internal point in an element can be obtained by means of Eq. (33).

4. THE SUBDOMAIN METHOD FOR NONLINEAR FUNCTIONALLY GRADED BI-MATERIALS

Consider the heat conduction problem in functionally graded bi-material that occupy the domains Ω_1 and Ω_2:

$$\sum_{i,j=1}^{2} \frac{\partial}{\partial X_i}\left(\tilde{K}_{ij}^{(l)}(\mathbf{X}, \mathrm{u}_l)\frac{\partial u_l(\mathbf{X})}{\partial X_j}\right) = 0 \qquad \forall \mathbf{X} \in \Omega_l, \qquad l = 1, 2, \tag{36}$$

where

$$\tilde{K}_{ij}^{(l)}(\mathbf{X}, \mathrm{u}_l) = \alpha_l(u_l)K_{ij}^{(l)}\exp(2\boldsymbol{\beta}^{(l)}\cdot\mathbf{X}) = \alpha_l(u_l)K_{ij}^{*(l)}. \tag{37}$$

As was done in (5), the Kirchhoff transformations are conducted in Ω_1 and Ω_2 as:

$$\begin{aligned} \Psi^{(1)}(u_1) &= \textstyle\int \alpha_1(u_1)du \qquad \forall \mathbf{X} \in \Omega_1 \\ \Psi^{(2)}(u_2) &= \textstyle\int \alpha_2(u_2)du \qquad \forall \mathbf{X} \in \Omega_2. \end{aligned} \tag{38}$$

Therefore, after the Kirchhoff transformation, the heat conduction problem has to be solved in sub-domain Ω_1 and Ω_2, separately. Moreover, the continuities of temperature and normal heat flow are required on the interface.

Making use of the hybrid graded element formulation on each sub-domain, we have:

$$[K^{(l)}]\{\Psi^{(l)}\} = \{g^{(l)}\}, \tag{39}$$

with

$$\left\{\Psi^{(l)}\right\} = \left\{\Psi_1^{(l)}\Psi_2^{(l)}\ldots\Psi_{N_S}^{(l)}\right\}, \ \left\{g^{(l)}\right\} = \left\{g_1^{(l)}g_2^{(l)}\ldots g_{N_S}^{(l)}\right\} \quad l = 1, 2, \tag{40}$$

where the superscript (l) stands for variables associated with the sub-domain Ω_l, and N_S is the number of the nodes in each sub-domain.

On the interface boundary Γ_I, the following conditions must be satisfied:

$$\begin{aligned} \left\{u_I^{(1)}\right\} &= \left\{u_I^{(2)}\right\} \\ \left\{q_I^{(1)}\right\} &= -\left\{q_I^{(2)}\right\} \end{aligned}, \tag{41}$$

where subscripts I represent the interface boundary between sub-domain Ω_1 and Ω_2. It should be mentioned that the field variables are $\Psi^{(i)}(i = 1, 2)$ in Eq. (39) but the continuities conditions (41) are defined in terms of temperature u.

To establish the finite element formulation for the bi-material, the element discretization is done for sub-domains Ω_1 and Ω_2, separately (see Figure 5). There are overlapped nodes on the interface (in bold for the illustration in Figure 5). The overlapped

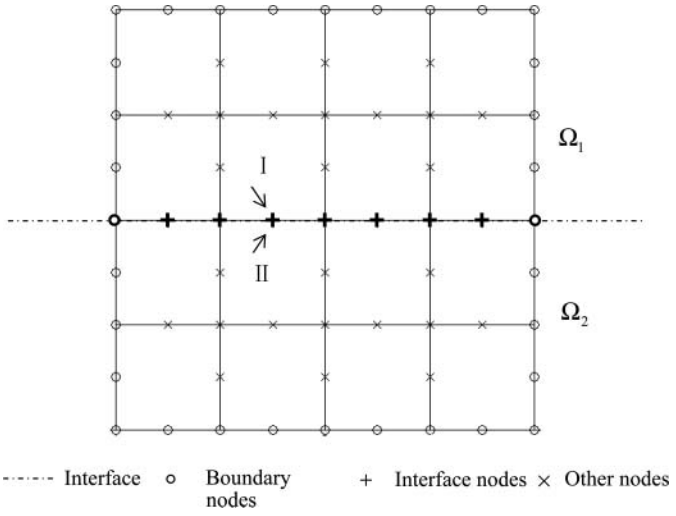

FIG. 5. Demonstration of element discretization and node types for the domain.

nodes have the same coordinate but belong to a different subdomain. We classify all the nodes in the whole domain into their types: boundary nodes whose temperatures are already known, interface nodes which locate on the interface, and the other nodes (see Figure 5). N_B, N_I, and N_O are the number of boundary nodes, interface nodes and other nodes, respectively ($N_B + N_I + N_O = N_S$).

Rearranging Eq. (39) according to the type of the nodes, we have:

$$\begin{aligned}\left[O^{(l)}\right]_{N_O\times N_O}\left\{\Psi_O^{(l)}\right\}_{N_O\times 1} &= -\left[B^{(l)}\right]_{N_O\times N_B}\left\{\Psi_B^{(l)}\right\}_{N_B\times 1} \\ -[I^I]_{N_O\times N_I}\left\{\Psi_I^{(l)}\right\}_{N_I\times 1} &\qquad l=1,2,\end{aligned} \tag{42}$$

where subscripts O, B, and I represent other node, boundary node, and interface node, respectively. The matrix **O**, **B**, and **I** can be formed by picking the corresponding entries k_{ij} from matrix **K**. The first term in the right hand side of the equation is known variables since the temperature at boundary nodes is prescribed (vector $\{\Psi_B^{(l)}\}$ is known). So the field variable of other nodes can be expressed in terms of the interface nodes by Eq. (42) in the form:

$$\left\{\Psi_O^{(l)}\right\} = -\left[O^{(l)}\right]^{-1}\left[B^{(l)}\right]\left\{\Psi_B^{(l)}\right\} - \left[O^{(l)}\right]^{-1}\left[I^I\right]\left\{\Psi_I^{(l)}\right\}, \tag{43}$$

that is $\Psi_O^{(l)} = f(\Psi_I^{(l)})$ for simplicity.

Using Eqs. (19), (20), and (32), we have:

$$q_e = -K_{eij}\frac{\partial u_e}{\partial X_j}n_i = -K^*_{eij}\frac{\partial \Psi_e}{\partial X_j}n_i = -\mathbf{A}\mathbf{K}^*_{\mathbf{e}}\mathbf{T}_e\mathbf{H}_e^{-1}\mathbf{G}_e\mathbf{d}_e, \tag{44}$$

where d_e consists of Ψ_B, Ψ_O, Ψ_I. Since Ψ_B is already known by the boundary condition and Ψ_O is the function of Ψ_I (see Eq. (42)), finally, d_e can be expressed in terms of Ψ_I. That is $d_e = f(\Psi_B, \Psi_O, \Psi_I) = f(\Psi_I)$. Substituting Eq. (44) to Eq. (41), a $2 \times N_I$ nonlinear equation for $\Psi_I^{(l)}$ ($l = 1, 2$) can be obtained:

$$\begin{aligned}&\psi^{-1}\left(\Psi_I^{(1)}\right) = \psi^{-1}\left(\Psi_I^{(2)}\right) \\ &\quad - \mathbf{A}^{(1)}\mathbf{K}^{*(1)}_{\mathbf{e}}\mathbf{T}_e^{(1)}\mathbf{H}_e^{(1)-1}\mathbf{G}_e^{(1)} f\left(\Psi_I^{(1)}\right) = \mathbf{A}^{(2)}\mathbf{K}^{*(2)}_{\mathbf{e}}\mathbf{T}_e^{(2)}\mathbf{H}_e^{(2)-1} \\ &\quad \times \mathbf{G}_e^{(2)} f(\Psi_I^{(2)}),\end{aligned} \tag{45}$$

$\Psi_I^{(l)}$ can be determined by solving nonlinear equations (45). Once $\Psi_I^{(l)}$ are obtained, $\Psi_O^{(l)}$ will be determined by Eq. (42), then all of the field variables $bm\Psi$ can be determined for each sub-domain. Finally, the temperature u in the whole domain can be found by $u = \psi^{-1}(\Psi)$.

5. NUMERICAL ASSESSMENTS

In order to evaluate the performance of the proposed approach, here we consider three typical benchmark problem, which are taken from Reference [11], for steady-state heat transfer in 2-D functionally nonlinear graded material and the results are compared with the analytical ones. These examples cover the cases that thermal conductivity is a linear function of temperature (example 1) and exponential function of temperature (example 2). The functionally graded bi-materials plate is studied in example 3, which covers three cases that are, respectively, two linear materials, two nonlinear materials with the same nonlinear term, and two nonlinear materials with different nonlinear terms.

In the calculation, to provide a more quantitative understanding on the accuracy of the results, the normalized error on a variable f is introduced as:

$$err(f(X)) = \frac{\left|f^{(num)}(X) - f^{(an)}(X)\right|}{\max\limits_{x\in\Omega}\left|f^{(an)}(X)\right|} \times 100\% \quad X \in \Omega, \tag{46}$$

where $f^{(num)}$ and $f^{(an)}$ are the numerical and exact result of the field variable.

Example 1. *The thermal conductivity being a linear function of temperature:*

A single nonlinear anisotropic FGM material square plate is considered. Its dimension is $\Omega = (-1, 1)\times(-1, 1)$. The thermal conductivity is a linear function of temperature:

$$\alpha(u) = 1 + \gamma u, \tag{47}$$

where γ is a constant. In the calculation, $K_{11} = 2.0$, $K_{12} = K_{21} = 0.0$, and $K_{22} = 1.0$. $\beta_1 = 0$, $\beta_2 = 1$ (heat conductivity varies along direction X_2 only), $\gamma = 0.5$ are used. 2×2 8-node quadrilateral elements are employed to model the solution domain.

Under Kirchhoff transformation, we obtain:

$$\Psi(u) = \int \alpha(u)du = \int (1+\gamma u)du = u + \frac{1}{2}\gamma u^2. \quad (48)$$

Since $\alpha(u) > 0$, the function Ψ is inverted such that taking only the positive root of Eq. (48):

$$u^{(nu)} = \frac{-1+\sqrt{1+2\gamma\Psi}}{\gamma}, \quad (49)$$

and the heat flux is

$$q^{(nu)}(\mathbf{X}) = -\sum_{i,j=1}^{2} \tilde{K}_{ij}\frac{\partial u(\mathbf{X})}{\partial X_j}n_i(\mathbf{X}) = -\sum_{i,j=1}^{2} K_{ij}\frac{\partial \Psi(\mathbf{X})}{\partial X_j}n_i(\mathbf{X})\exp(2\beta\cdot\mathbf{X}). \quad (50)$$

When $\gamma = 0.5$, the analytical solution is [11]:

$$u^{(an)}(\mathbf{X}) = 2\sqrt{\Psi(\mathbf{X})+1} - 2, \quad \mathbf{X}\in\Omega, \quad (51)$$

where

$$\Psi(\mathbf{X}) = \frac{\sqrt{1-c/p}}{\sqrt{2p}}\sinh(p)e^{-X_2}, \quad \mathbf{X}\in\Omega, \quad (52)$$

$$c = X_1/\sqrt{2} - 1, \quad p = \sqrt{c^2+X_2^2}. \quad (53)$$

Moreover, the analytical solution for heat flux is obtained by taking the normal derivative of the analytical solution with respect to coordinates and is given by:

$$q^{(an)}(\mathbf{X}) = -e^{2X_2}\left\{2\frac{\partial\Psi(\mathbf{X})}{\partial X_1}n_1(\mathbf{X}) + \frac{\partial\Psi(\mathbf{X})}{\partial X_2}n_2(\mathbf{X})\right\}, \quad \mathbf{X}\in\Omega, \quad (54)$$

where

$$\begin{cases} \dfrac{\partial\Psi(\mathbf{X})}{\partial X_1} = \dfrac{e^{-X_2}}{2p\sqrt{p}}\left[\left(\dfrac{(c/p)^2-1}{2\sqrt{1-c/p}} - \dfrac{c\sqrt{1-c/p}}{2p}\right)\sinh(p) + c\sqrt{1-c/p}\cosh(p)\right] \\ \dfrac{\partial\Psi(\mathbf{X})}{\partial X_2} = \dfrac{e^{-X_2}}{\sqrt{2p}}\left[\left(\dfrac{cX_2}{2p^3\sqrt{1-c/p}} - \dfrac{X_2\sqrt{1-c/p}}{2p^2} - \sqrt{1-c/p}\right)\sinh(p) + \frac{X_2\sqrt{1-c/p}}{p}\cosh(p)\right] \end{cases} \quad (55)$$

In our analysis, the Direchlet boundary conditions are considered:

$$u(\mathbf{X}) = f(\mathbf{X}), \quad \mathbf{X}\in\partial\Omega. \quad (56)$$

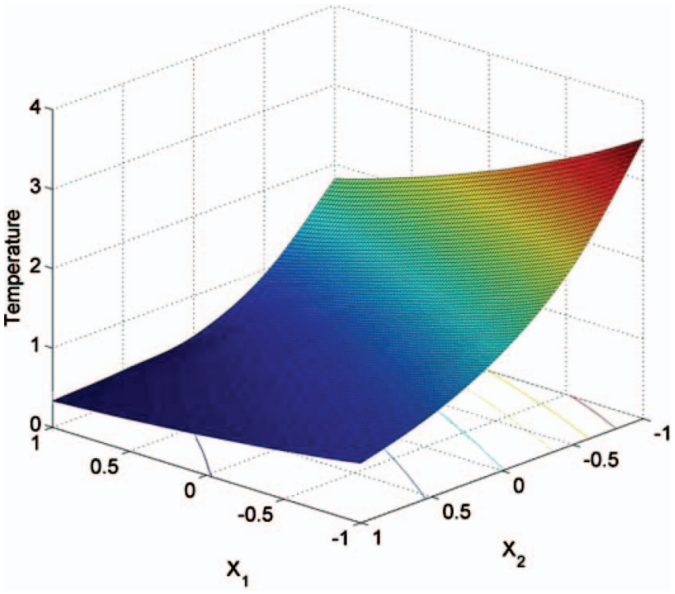

FIG. 6a. Temperature distribution for Example 1. (Color figure available online.)

Under Kirchhoff transformation and assuming $\gamma = 0.5$, the condition remains a Dirichlet condition for Ψ and is given by

$$\Psi(\mathbf{X}) = f(\mathbf{X}) + \frac{1}{4}f^2(\mathbf{X}), \quad \mathbf{X}\in\partial\Omega. \quad (57)$$

Figure 6a illustrates the temperature distribution in the FGM plate and Figure 6b shows the corresponding isothermal distribution. It can be seen that the numerical solution matches

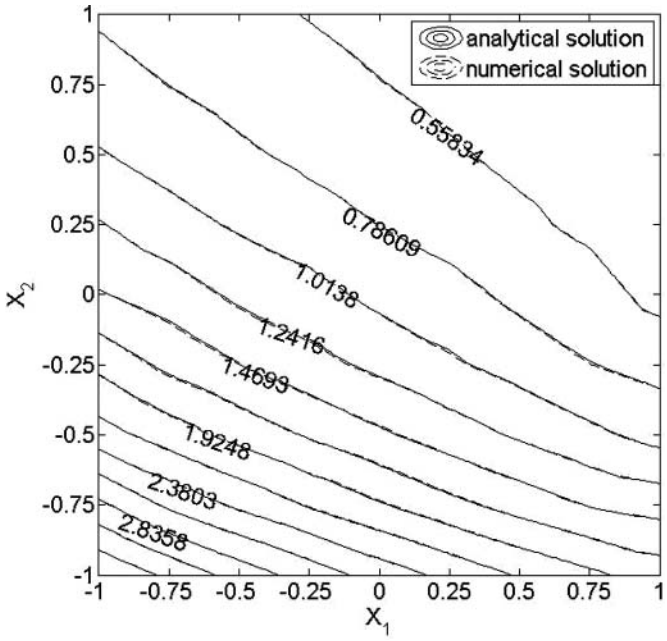

FIG. 6b. Isothermals for Example 1.

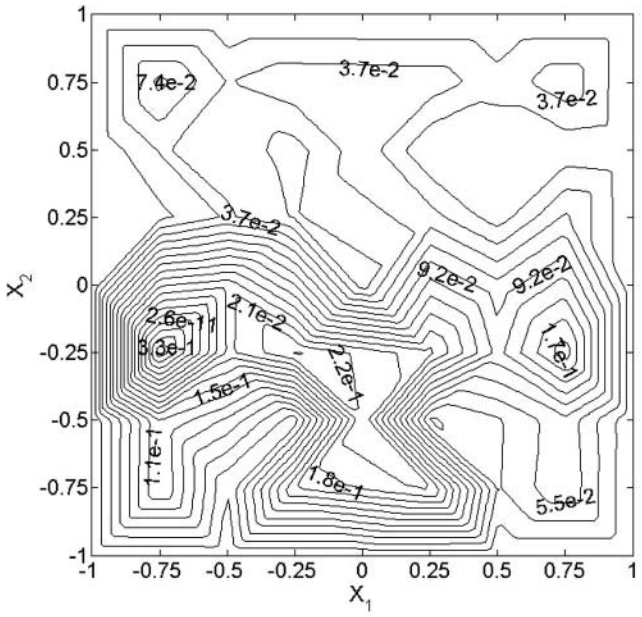

FIG. 7a. Percentage of normalized error distribution for temperature (by Kirchhoff transformation) for Example 1.

very well with the analytical solution. The calculation is also conducted by an iterative method and convergence is achieved using 31 iterations. The corresponding percentage of normalized error distributions by these two methods are presented in Figures 7a and 7b, respectively. Comparing Figure 7b with 7a, the error level in the iterative method is higher than that in the Kirchhoff transformation method. It indicates that the results

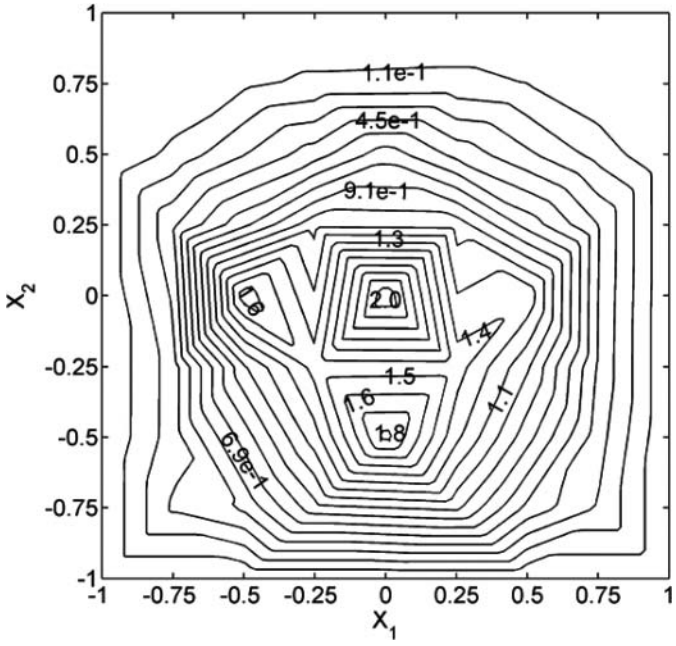

FIG. 7b. Percentage of normalized error distribution for temperature (by iterative method) for Example 1.

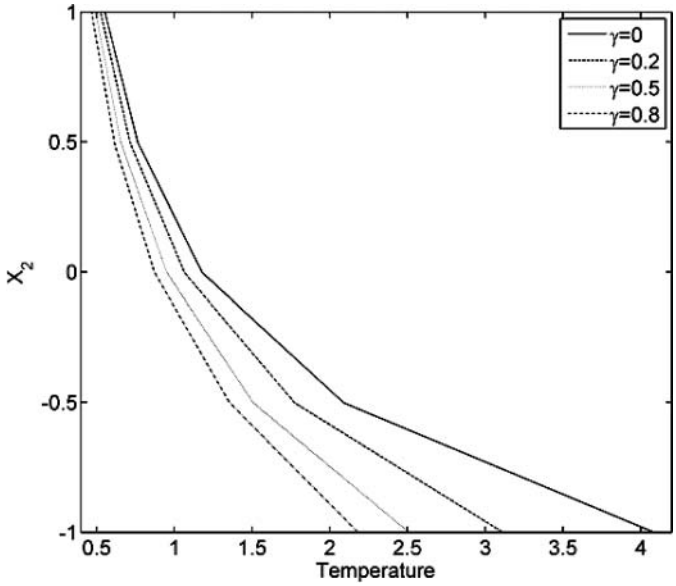

FIG. 8. Temperature distribution at $X_1 = 0$ with different γ.

from the Kirchhoff transformation method are more accurate than those from the iterative method. In addition, to assess the effect of linear coefficient, $\gamma = 0, 0.2, 0.5, 0.8$ are employed in the calculation. Figure 8 shows the temperature distribution along direction X_2 ($X_1 = 0$), which is the graded direction with different γ. It can be seen from Figure 8 that the curve becomes more steep when γ becomes bigger.

Example 2. *The thermal conductivity being an exponential function of temperature:*

In this example, the thermal conductivity being an exponential function of temperature is considered:

$$\alpha(u) = e^u. \tag{58}$$

The discretization of the problem domain and other parameters are the same as those in Example 1.

Making use of the Kirchhoff transformation, we have

$$\Psi(u) = \int e^u du = e^u, \qquad u = \ln \Psi. \tag{59}$$

Its analytical solution is

$$u^{(an)}(\mathbf{X}) = \ln(\Psi(\mathbf{X})) = \ln\left(\frac{\sqrt{1 - c/p}}{\sqrt{2p}} \sinh(p) e^{-X_2}\right), \tag{60}$$

where c and p are defined in Eq. (53).

Figure 9a shows the temperature distribution in the FGM plate. We can see that the lowest temperature occurs at the corner (1,1), then increases gradually along a diagonal direction

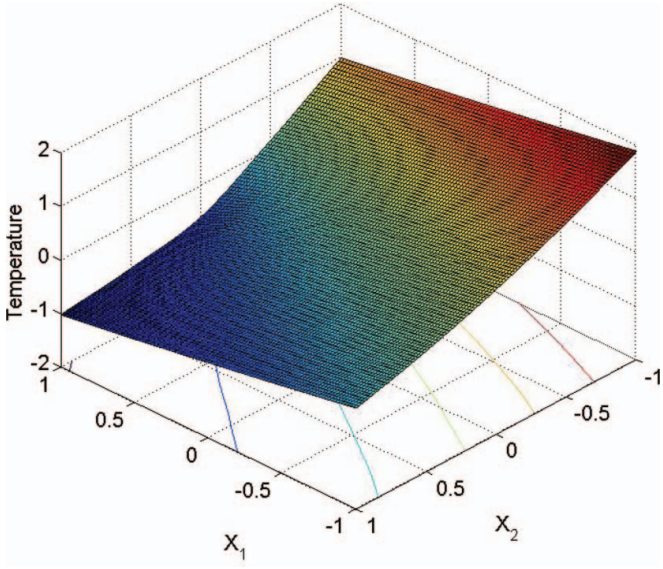

FIG. 9a. Temperature distribution for Example 2. (Color figure available online.)

and reaches the highest value at the corner $(-1,-1)$. Figure 9b illustrates isothermal distribution of the FGM plate. It can be seen from Figure 9b that the numerical solution is in excellent agreement with the analytical solution. The calculation is also conducted by the iterative method and the convergence is achieved using 16 iterations. Figures 10a and 10b illustrate the corresponding percentage of normalized error distributions from Kirchhoff transformation method and iterative method, respectively. It can be seen from Figure 10 that the Kirchhoff transformation method can again achieve more accurate results than those from the iterative method. The reason might be that the error is accumulated by each iteration step in the iterative

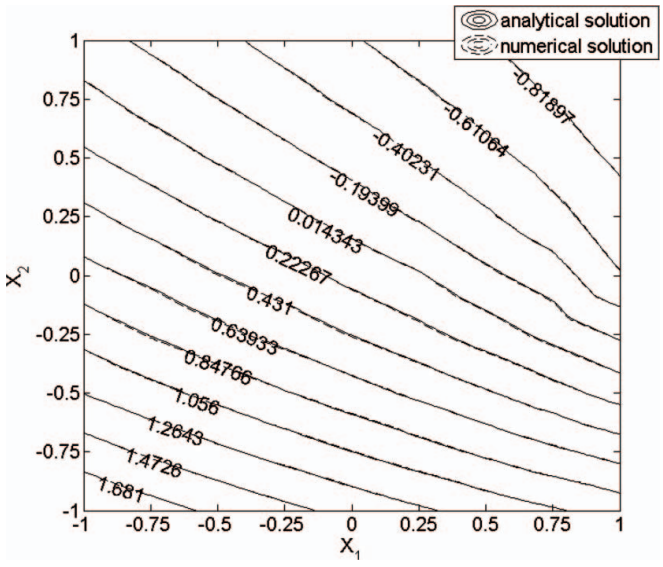

FIG. 9b. Isothermals for Example 2.

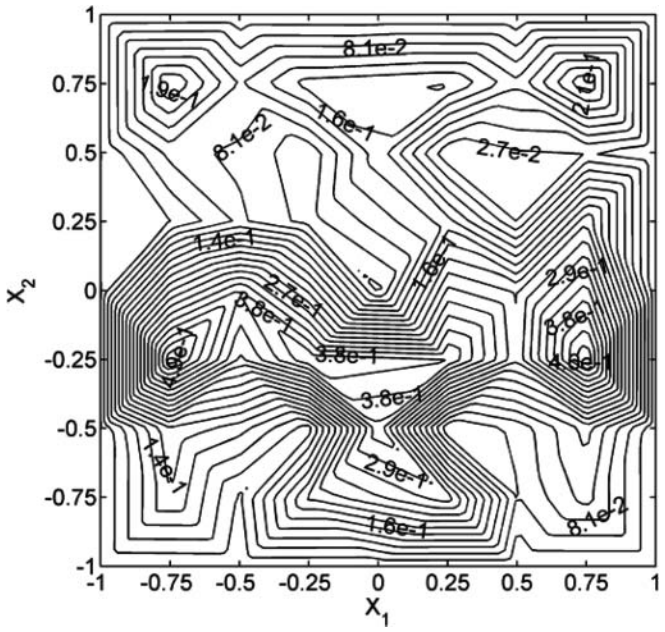

FIG. 10a. Percentage of normalized error distribution for temperature (by Kirchhoff transformation) for Example 2.

method. Further, the choice of initial value and convergent criterion can also affect the accuracy of the results. In addition, the iterative method needs more computing time because of the complex iterative process. Therefore, the performance of the Kirchhoff transformation method is more stable, accurate, and time-saving than the iterative method. We choose the Kirchhoff transformation method in the following numerical simulation.

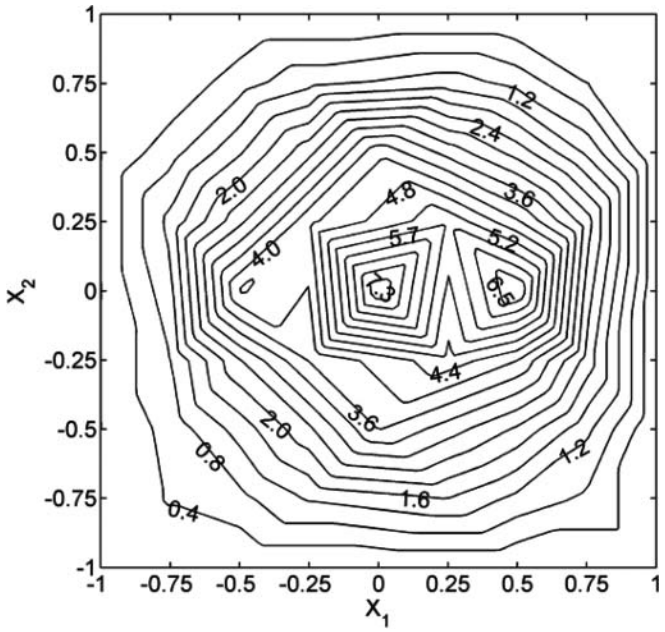

FIG. 10b. Percentage of normalized error distribution for temperature (by iterative method) for Example 2.

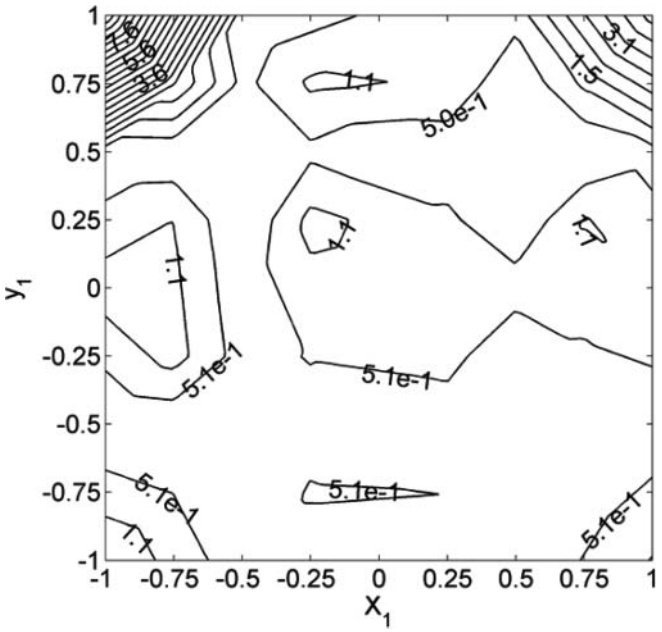

FIG. 11a. Percentage of normalized error distribution for heat flux q_1.

The percentage of normalized error for heat flux in direction X_1 and X_2 are shown in Figures 11a and 11b, respectively. It can be seen from these two figures that the proposed model yields high accuracy for the heat flux field as well.

Example 3. *Functionally graded bi-materials:*

A bi-material of FGM with the solution domain $\Omega = \Omega_1 \cup \Omega_2$ is considered, where $\Omega_1 = (-1, 1) \times (0, 1)$ and $\Omega_2 = (-1, 1) \times (-1, 0)$ represent the domains occupied by the two materials. In the calculation, $\boldsymbol{\beta}^{(1)} = (1, 1)$, $\boldsymbol{\beta}^{(2)} = (1, 2)$, $K_{11} = 2.0$, $K_{12} = K_{21} = 0.0$, and $K_{22} = 1.0$ are used and Direchlet boundary conditions $u_l = \exp(-2\boldsymbol{\beta}^{(l)} \cdot \mathbf{X})$, $\mathbf{X} \in \Omega_l$, $l = 1, 2$ are enforced on the four edges of the plate. 4×2 8-node quadrilateral elements are employed to model each sub-domain. Three different kinds of functionally graded bi-materials plates are investigated in this example, which almost covers all types of bi-materials.

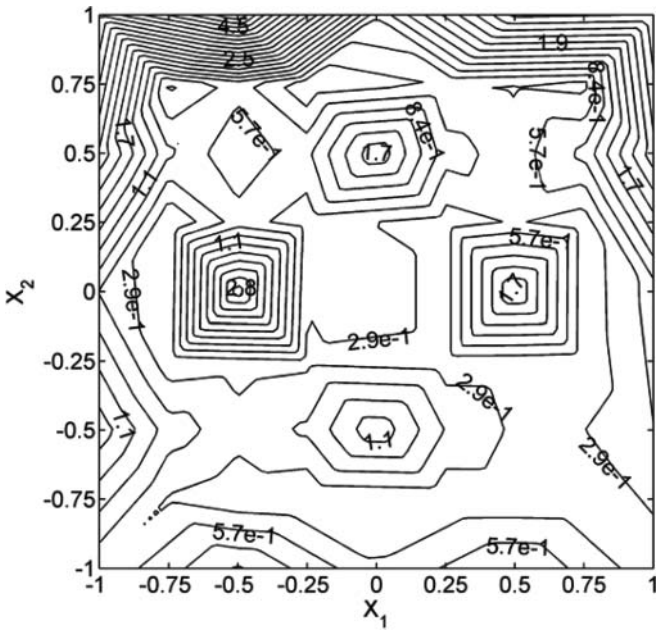

FIG. 11b. Percentage of normalized error distribution for heat flux q_2.

Case 1. Two linear materials

For the two linear materials, $\alpha_1(u_1) = \alpha_2(u_2) \equiv 1$. The analytical solutions for the temperature are [11]:

$$u_l^{(an)} = \exp\big(-2\beta^{(l)} \cdot \mathbf{X}\big), \qquad \mathbf{X} \in \Omega_l \quad l = 1, 2. \tag{61}$$

Figure 12a illustrates the isothermals in the linear bi-materials FGM plate and Figure 12b presents the corresponding percentage of normalized error distribution. It can be seen that the numerical solution agrees with the analytical solution very well.

Case 2. Two nonlinear materials with the same nonlinear term

In this case, a two nonlinear material FGM plate with the same nonlinear term $\gamma = 0.5$ is considered.

Figure 13 shows the isothermal distributions in the nonlinear bi-material FGM plate. It can be seen through comparing with Figure 12a that the isothermals of case 2 are curlier than those of case 1 due to the nonlinear term of the heat conductivity.

Case 3. Two nonlinear materials with different nonlinear terms

For the two nonlinear materials in a FGM plate with different nonlinear terms, here, $\gamma_1 = 0.5, \gamma_2 = 0.2$ are used. Kirchhoff

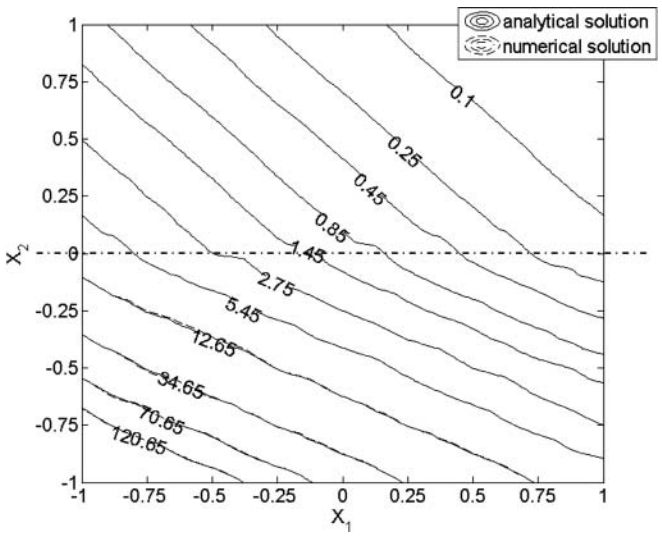

FIG. 12a. Numerical of isothermals for two linear FGMs for Example 3.

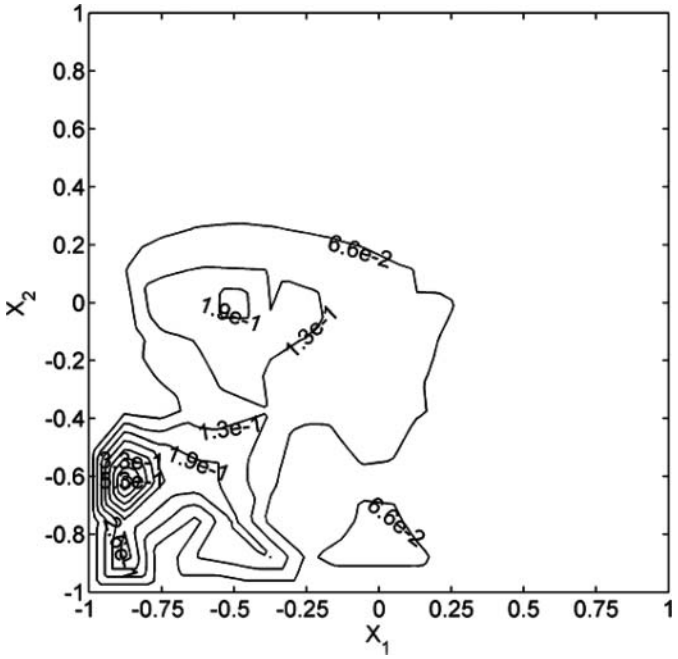

FIG. 12b. Percentage of normalized error distribution for temperature for Example 3.

transformation is conducted in the two sub-domains Ω_1 and Ω_2, and are written as:

$$\Psi_1(u) = u + \frac{1}{4}u^2, \quad \Psi_1 \in \Omega_1,$$
$$\Psi_2(u) = u + \frac{1}{10}u^2, \quad \Psi_2 \in \Omega_2.$$

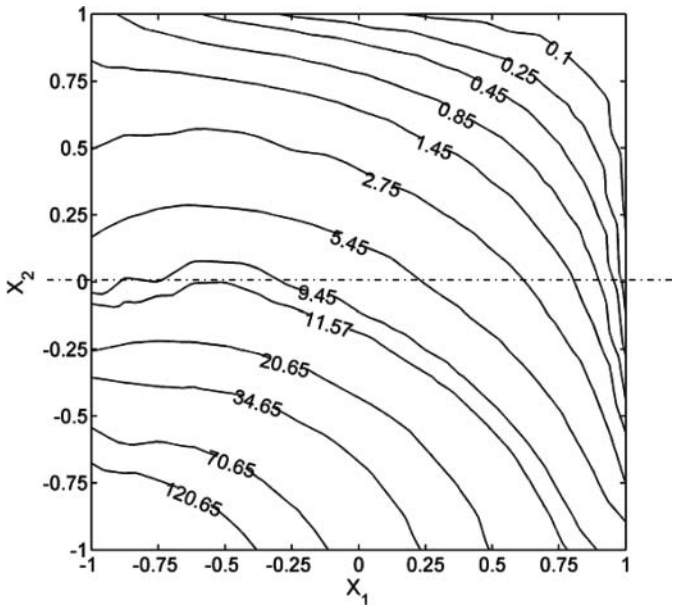

FIG. 13. Isothermals for two nonlinear FGMs with the same nonlinear term.

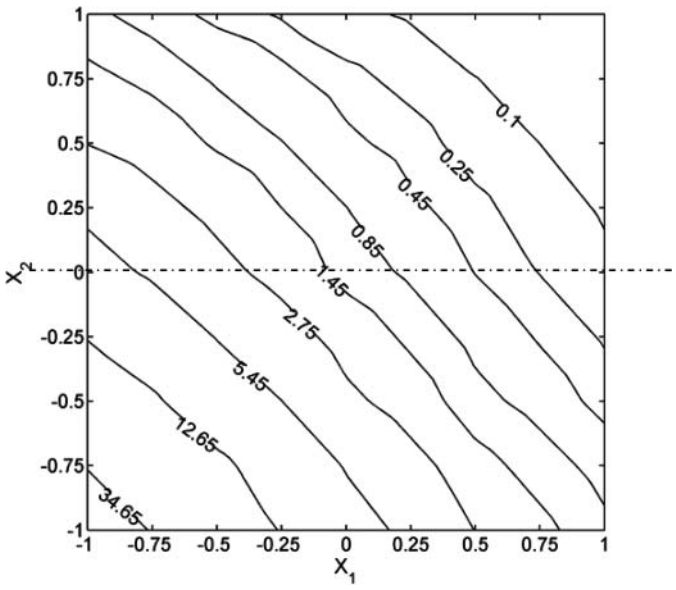

FIG. 14. Isothermals for two nonlinear FGMs with different nonlinear terms.

The method introduced in Section 4 is employed to solve the problem. It should be mentioned that the temperature continuity on the interface is $2\sqrt{1+\Psi_1}-2 = 5\sqrt{1+0.4\Psi_2}-5$. Figure 14 illustrates isothermal distributions in the nonlinear bi-materials FGM plate with different nonlinear terms. It can be seen that the temperature level is lower than the previous two cases and the isothermals are more straight than that in Figure 13, since the smaller nonlinear coefficient ($\gamma_2 = 0.2$) was used in this case. Figure 15 compares the temperature distribution on the interface for the three cases. For cases 1 and 3, the temperature

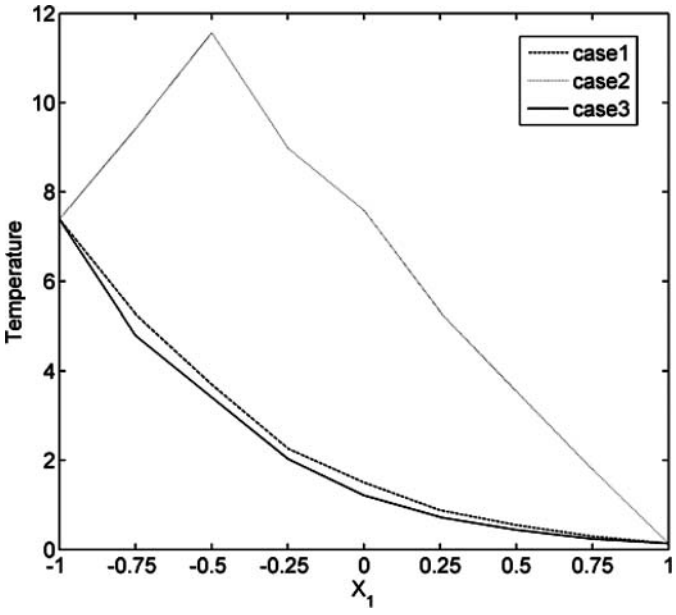

FIG. 15. Temperature distribution along the interface for the three cases.

monotone decreased along the interface. We also can observe this trend from Figures 12a and 14 that the isothermals (valued 5.45, 2.75, 1.45, 0.85, 0.45, 0.25, 0.1) go through the interface. But for case 2, the temperature on the interface goes up, reaches the peak value 11.57, and then decreases. It can also be seen from Figure 13 that the isothermal valued 11.57 is tangent to the interface and some isothermals, like the one valued 9.45, cross the interface twice.

6. CONCLUSIONS

In this article, both the Kirchhoff transformation and iterative method are used to deal with the nonlinear term for heat conduction problem of the nonlinear functionally graded materials. A 2-D hybrid graded element model is developed for analyzing thermal behavior of nonlinear FGMs. In the present model, the graded elements, which incorporate the material property gradient at the element level, have been presented in an internal element domain. A linear combination of the fundamental solution at points outside the element domain is used to approximate the field variable in the internal element domain, and the boundary interpolation functions are used to construct the frame field. Moreover, the multi-subdomain method is developed to deal with the bi-material problem. Several typical examples are considered to evaluate the performance of the proposed method. The results indicate that the graded element model can simulate the graded material naturally and conveniently and the Kirchhoff transformation is very effective to deal with the nonlinear material property. It should be mentioned that the Kirchhoff transformation used in this article may have some limitations. For example, it may be difficult for multi-material problems with different nonlinear terms, because different transformations are used for different material domains, which makes the problem more complicated. This can be compensated by using the multi-subdomain method introduced in this article.

REFERENCES

1. G. Anlas, M.H. Santare, and J. Lambros, Numerical calculation of stress intensity factors in functionally graded materials, Int. J. Fract., vol. 104, pp. 131–143, 2000.
2. H. Li, J. Lambros, B.A. Cheeseman, and M.H. Santare, Experimental investigation of the quasi-static fracture of functionally graded materials, Int. J. Solids Struct., vol. 37, pp. 3715–3732, 2000.
3. P. Gu, M. Dao, and R.J. Asaro, A simplified method for calculating the crack-tip field of functionally graded materials using the domain integral, J. Appl. Mech., vol. 66, pp. 101–108, 1999.
4. M.H. Santare and J. Lambros, Use of graded finite elements to model the behavior of nonhomogeneous materials, J. Appl. Mech., vol. 67, pp. 819–822, 2000.
5. J.H. Kim and G.H. Paulino, Isoparametric graded finite elements for nonhomogeneous isotropic and orthotropic materials, J. Appl. Mech., vol. 69, pp. 502–514, 2002.
6. F.Y. Chen and W.Q. Jie, Finite element design of MgO/Ni system functionally graded materials, J. Mater. Process. Technol., vol. 182, pp. 181–184, 2007.
7. G. H. Paulino, A. Sutradhar, and L.J. Gray, Boundary element method for functionally graded materials. In: International Association for Boundary Element Methods, University of Texas–Austin, Austin, Texas, 2002.
8. A. Sutradhar and G.H. Paulino, The simple boundary element method for transient heat conduction in functionally graded materials, Comput. Meth. Appl. Mech. Eng, vol. 193, pp. 4511–4539, 2004.
9. J. Wen and M.M. Khonsari, Transient heat conduction in rolling/sliding components by a dual reciprocity boundary element method, Int. J. Heat Mass Transfer, vol. 52, pp. 1600–1607, 2009.
10. Y. Ochiai, Two-dimensional steady heat conduction in functionally gradient materials by triple-reciprocity boundary element method, Eng. Anal. Bound. Elem., vol. 28, pp. 1445–1453, 2004.
11. H. Wang, H. Qin, and Y.L. Kang, A new meshless method for steady-state heat conduction problems in anisotropic and inhomogeneous media, Arch. Appl. Mech., vol. 74, pp. 563–579, 2005.
12. H. Wang and Q.H Qin, Meshless approach for thermo-mechanical analysis of functionally graded materials, Eng. Anal. Bound. Elem., vol. 32, pp. 704–712, 2008.
13. X.H. Wu and W.Q Tao, Meshless method based on the local weak-forms for steady-state heat conduction problems, Int. J. Heat Mass Transfer, vol. 51, pp. 3103–3112, 2008.
14. J. Sladek, V. Sladek, and C.H. Zhang, Transient heat conduction analysis in functionally graded materials by the meshless local boundary integral equation method, Comput. Mater. Sci., vol. 28, pp. 494–504, 2003.
15. H. Wang and Q.H. Qin, Fundamental-solution-based finite element model for plane orthotropic elastic bodies, Eur. J. Mech. A. Solids, vol. 29, pp. 801–809, 2010.
16. H. Wang and Q.H. Qin, Hybrid FEM with fundamental solutions as trial functions for heat conduction simulation, Acta Mech. Solida Sin., vol. 22, pp. 487–498, 2009.
17. Q.H. Qin and H. Wang, MATLAB and C Programming for Finite Element Methods, CRC Press, Taylor & Francis Group LLC, Boca Raton, FL, 2008.
18. Q.H. Qin, The Trefftz Finite and Boundary Element Method, WIT Press, Southampton, MA, 2000.
19. Q.H. Qin, Hybrid Trefftz finite-element approach for plate bending on an elastic foundation, Appl. Math. Model., vol. 18, pp. 334–339, 1994.
20. Q.H. Qin, Nonlinear analysis of Reissner plates on an elastic foundation by the BEM, Int. J. Solids Struct., vol. 30, pp. 3101–3111, 1993.
21. J.R. Berger, P.A. Martin, V. Mantič, and L.J. Gray, Fundamental solutions for steady-state heat transfer in an exponentially graded anisotropic material, Zeitschrift für Angewandte Mathematik und Physik (ZAMP), vol. 56, pp. 293–303, 2005.
22. L.J. Gray, T. Kaplan, J.D. Richardson, and G.H. Paulino, Green's functions and boundary integral analysis for exponentially graded materials: Heat conduction, J. Appl. Mech., vol. 70, pp. 543–549, 2003.
23. Q.H. Qin, Variational formulations for TFEM of piezoelectricity, Int. J. Solids Struct., vol. 40, pp. 6335–6346, 2003.
24. H. Wang, Q.H. Qin, and Y.L. Kang, A meshless model for transient heat conduction in functionally graded materials, Comput. Mech., vol. 38, pp. 51–60, 2006.
25. H. Wang and Q.H. Qin, A meshless method for generalized linear or nonlinear Poisson-type problems, Eng. Anal. Bound. Elem., vol. 30, pp. 515–521, 2006.